## EDGE ARTICLE

Check for updates

# Multiple functional bulk passivator pyrimidine derivative stabilizing perovskite precursors for efficient carbon-based perovskite solar cells

Mengqi Geng,[a] Jialiang Li,[a] Ke Wang, [b] Le Jiang,[a] Dan Lu,[a] Shoaib Iqbal,[a] Yu Gu,[a] Lixin Chen [a] and Tingting Xu [*ac]

Over the past few decades, perovskite solar cells (PSCs) have attracted great research attention attributed to their promising future as alternative energy sources. Even with exceptionally high power conversion efficiency (PCE) up to 27.3%, the chemical instability of perovskite precursors, induced by the undesirable transition of $[PbI_6]^{4-}$ octahedron and the high volatility of organic cations, is a big obstacle in achieving high efficiency and superior long-term stability of PSCs, thus restricting their industrial production and practical application. Herein, the stability of perovskite precursor solution was modulated by introducing a multifunctional passivator: ethyl-4-amino-2-mercapto-5-pyrimidinecarboxylate (AMPM). AMPM with electron-donating and electron-accepting groups can interact with perovskite precursor through coordination and hydrogen bonds. Thus, it effectively dissociates face- and edge-shared $[PbI_6]^{4-}$ octahedral aggregates, enhancing precursor colloidal dispersion, improving precursor stability and driving a reorganization into corner-shared $[PbI_6]^{4-}$. Additionally, AMPM preferentially increases the relative abundance of higher-Miller-index (220) and (310) planes while preserving the predominance of the primary (110) facet, thereby reducing perovskite defect state density and improving charge extraction. As a result, compared with the control carbon-based PSCs (C-PSCs), the champion PCE of the C-PSCs was increased up to 18.48% *via* AMPM treatment in perovskite bulk films. The PCE of the AMPM-treated C-PSCs retained 90% of the initial value after storage at 30–40% relative humidity for 50 days, compared with that of less than 47% for the original device. This research provides a novel approach to fabricate high-performance and durable perovskite-based optoelectronic devices by tuning the properties of the precursor materials *via* colloidal chemistry.

## 1. Introduction

Organic–inorganic lead halide hybrid perovskite solar cells (PSCs) have garnered unprecedented attention due to their exceptional optoelectronic properties, including high absorption coefficients,[1,2] tunable bandgaps,[3,4] high carrier mobility,[2,5] and bipolar charge transport.[6,7] The power conversion efficiency (PCE) of PSCs has dramatically improved from 3.8%[8] in 2009 to the current 27.3%,[9] pushing them to the forefront of competitive and promising photovoltaic technologies. Perovskite films are generally prepared by solution processing, in which multiple components such as halides ($PbI_2$, MAI, CsI and FAI) are dissolved in a mixed solution to form a precursor solution.

The as-formed precursor consists of colloidal particles self-assembled from face-/edge-/corner-sharing $[PbI_6]^{4-}$ octahedra and organic/inorganic cations.[10] Previous reports showed that dimethylformamide (DMF) or dimethylsulfoxide (DMSO) solvent can form an intermediate adduct with the colloidal particles to reach chemical equilibrium and play a key role in subsequent perovskite crystallization.[11,12] Crucially, this solute–solvent equilibrium remains reversible, rendering the system inherently labile.[13] This instability, driven by the high volatility of organic cations and the transformation of $[PbI_6]^{4-}$ octahedral connectivity, favors the formation of a perovskite film with a high defect state density.[14–16] Moreover, DMF hydrolysis yielding dimethylamine can induce methylamine cation ($MA^+$) deprotonation, causing the precursor composition to deviate further from the expected values.[17] Thus, the characteristics of the perovskite precursor inevitably compromise the performance and stability of PSCs. In order to improve the quality of perovskite films, multifunctional passivators are commonly added into the perovskite precursor to passivate film defects in the bulk. The effect of passivators interacting with perovskite film is often studied after crystallization, while how

*aSchool of Chemistry and Chemical Engineering, Northwestern Polytechnical University, Xi'an, Shaanxi 710129, China. E-mail: tingtingxu@nwpu.edu.cn*

*bFrontiers Science Center for Flexible Electronics (FSCFE), Shaanxi Institute of Flexible Electronics (SIFE) & Shaanxi Institute of Biomedical Materials and Engineering (SIBME), Northwestern Polytechnical University (NPU), Xi'an, Shaanxi 710072, China*

*cShenzhen Research Institute of Northwestern Polytechnical University, Shenzhen, Guangdong 518057, China*

the passivators cooperate with the perovskite precursor solution is rarely reported. Therefore, there is an urgent need to understand not only how to passivate the perovskite film, but also how the passivator affects the stability of the precursor solution.

In bulk passivation, various additive engineering is adopted to manipulate the precursor solution.[18–20] Additives containing electron-donating or electron-accepting functional groups can interact with the uncoordinated ions in perovskites through coordination bonds, electrostatic interactions, or hydrogen bonds.[21–26] These interactions are beneficial for regulating the coordination chemistry of the perovskite precursor and thus control the crystallization pathways.[27,28] For instance, Gou et al. used piperazine-2-carboxylic acid dihydrochloride additives to inhibit $MA^+$ deprotonation by forming strong two-point hydrogen bonds, thereby extending the shelf life of the perovskite precursor solution.[29] Hu et al. also employed reductive additives to inhibit the degradation reaction between methylamine (MA) and formamidine (FA) by consuming iodine ($I_2$) by-products and suppressing the deprotonation of $MA^+$, stabilizing the perovskite precursor solution.[30] Yin et al. utilized synergistic $H^+/I^-$ oxidation coupled with reductive peroxyacetic acid, achieving rapid equilibrium in MA/FA assembly for FA-dominant perovskites with exceptional solution stability.[31] Tian et al.[32] and Jeon et al.[33] applied colloidal state control through ionic bond strength modulation, concurrently suppressing ink degradation and enabling preferential growth of macroscopic crystals. Wang et al. developed a MA-based gel precursor in an acetonitrile dispersion system.[34] Owing to the highly volatile nature of the acetonitrile-based gel perovskite precursor solution and its abundant high-valent $PbI_n^{2-n}$ coordination compounds, the uniformity and quality of perovskite films were enhanced. Despite these advances, the mechanistic links between passivation molecule interactions in perovskite precursor solutions and their subsequent regulation of colloidal assembly, precursor stabilization, and defect-minimized crystallization dynamics are not fully understood.

In this work, we propose a feasible strategy to modulate a perovskite precursor and regulate its crystallization growth using a multifunctional passivator: ethyl-4-amino-2-mercapto-5-pyrimidinecarboxylate (AMPM). To the best of our knowledge, this is the first time that AMPM with functional groups of amino (–NH₂), mercapto (–SH), pyrimidine N, and ester groups has been used to adjust a perovskite precursor solution. The multifunctional groups of AMPM efficiently attach to the face- and edge-shared $[PbI_6]^{4-}$ octahedra through coordination and hydrogen bonds, thereby enhancing the dispersion and stability of the precursor and forming the more stable corner-sharing $[PbI_6]^{4-}$ octahedra. Meanwhile, AMPM optimized crystal orientations of perovskites during growth, thereby reducing defect density and enhancing the charge transport and collection properties of perovskite films. As a result, the champion PCE of AMPM-modified carbon-based PSCs (C-PSCs) was increased to 18.48% using poly(3-hexylthiophene) (P3HT) hole transport layer (HTL) and a tea polyphenol-functionalized liquid metal Ga (TP@Ga)-modified carbon electrode. The unencapsulated devices retained 90% initial PCE after 50-day ambient storage (30–40% RH), demonstrating exceptional

operational stability. This study establishes molecularly engineered synchronization of precursor colloidal stability and crystallization kinetics as a scalable manufacturing platform, addressing reproducibility limitations in perovskite photovoltaics. The methodology shows particular promise for industrial ink formulation enabling high-throughput PSC production.

## 2. Experiment section

### 2.1 Fabrication of carbon-based perovskite solar cells

Perovskite precursor solutions were formulated as per established methodology by co-dissolving methylammonium iodide (MAI, 159 mg, >99.5%, Xi'an p-OLED) and lead iodide (PbI₂, 461 mg, >99.99%, Xi'an p-OLED) in a DMSO/DMF co-solvent system (0.07 : 0.64 mL, Macklin/Aladdin) under continuous agitation (35 °C, overnight).[35] For PSC fabrication, a multi-layer nanocrystalline TiO₂ film was formed on cleaned FTO glass to serve as the electron transport layer (ETL). The perovskite precursor solution was then spin-coated onto the ETL at 4000 rpm for 20 seconds, with ether rapidly added as an anti-solvent. The film was subsequently annealed at 95 °C for 10 minutes to enhance crystallization. For passivated PSCs, AMPM was incorporated into the precursor solution (0.711 mL) at concentrations between 0 and 2 mg. A 10 mg L⁻¹ P3HT solution in isopropanol (IPA) was spin-coated at 3000 rpm for 30 seconds and annealed at 100 °C for 5 minutes to form the HTL. The TP@Ga-modified carbon electrode was fabricated according to our previous method.[36] Finally, commercial carbon paste was doctor bladed onto the perovskite surface and heated at 100 °C to complete the device. The solar cell's active area was 0.12 cm².

### 2.2 Characterizations

Computational modeling employed Gaussian 09 and Gauss-View 5.0 for molecular geometry optimization and electrostatic potential mapping. Solution-phase colloidal distributions were quantified via dynamic light scattering (DLS, nano laser analyzer). Surface topography was investigated by field-emission scanning electron microscopy (SEM) (Verios G4), while nanoscale electrical properties including contact potential difference were probed using atomic force microscopy (AFM)/Kelvin probe force microscopy (KPFM) (Bruker Dimension platforms). Electronic structure characterization combined ultraviolet photoemission spectroscopy (UPS) and X-ray photoelectron spectroscopy (XPS) (Axis Supra spectrometer) with UV-visible absorption spectroscopy (Hitachi U-3900 h). Photophysical properties were assessed through steady-state/time-resolved photoluminescence (PL/TRPL, PicoQuant FluoTime 300). Molecular interactions were verified by FTIR spectroscopy (Bruker Tensor II, 4000–400 cm⁻¹) and proton nuclear magnetic resonance (¹H NMR) (500 MHz, DMSO-$d_6$ solvent). Electrochemical properties including charge transfer kinetics were evaluated via electrochemical impedance spectroscopy (EIS) and Mott–Schottky (M–S) analysis (CHI 660 E, 1.0–1.2 V bias, 1 kHz). Trap density quantification utilized space charge limited current (SCLC) measurements in electron-only architectures (FTO/TiO₂/Perovskite/PCBM/Carbon). Photovoltaic

performance was benchmarked under AM 1.5 G illumination (Newport Class AAA solar simulator, 100 mW cm$^{-2}$ calibrated), recording the current density–voltage ($J$–$V$) curves (Keithley 2401) and stabilized power output at maximum power point. EQE spectra (300–800 nm, unbiased) were acquired using an Enli Tech QE system, with hydrophobicity characterized by contact angle goniometry (Krüss DSA25).

## 3. Results and discussion

The crystalline quality of perovskite films is critically dependent on the colloidal state of the precursor solution, such as its dispersion and stability, and the structural integrity of the fundamental $[PbI_6]^{4-}$.[37,38] Especially when a passivator is added into the perovskite precursor solution, it would largely affect its colloidal chemistry. To exert precise control over colloidal assembly and enhance the stability of $[PbI_6]^{4-}$ octahedra, multifunctional molecule AMPM was introduced into the perovskite precursor. The molecular structure and electrostatic potential (ESP) distribution of AMPM are shown in Fig. 1a. The negative ESP centers around the –NH$_2$ and ester (–O–) groups, while the positive ESP centers on the pyrimidine N, –SH, and carbonyl (–C=O) groups. These characteristics enabled AMPM to interact with MAI and PbI$_2$ precursors. They also show that AMPM has the ability to mitigate octahedral deformation, passivate defects and control crystal growth.

DLS was conducted to explore the effect of AMPM on the colloidal chemistry in perovskite precursor solution. As shown in Fig. 1b, the colloidal size reduced with increasing addition of

AMPM. The average colloidal sizes of perovskite precursor solutions of 0, 0.5, 1, 1.5 and 2 mg were 201, 180, 143, 105 and 76 nm, respectively (seen in Table S1). The reduction in colloidal size is attributed to the interactions of AMPM with perovskite precursors, which can effectively disrupt the photo-inactive face- and edge-sharing $[PbI_6]^{4-}$ aggregates and promote the formation of thermodynamically favored corner-sharing $[PbI_6]^{4-}$ octahedra.[14,39] This led to the enhancement in the dispersibility of the precursor solution. While reduced colloidal size promotes homogeneous nucleation and enlarges final grains through diminished nucleation density,[40–42] excessive size reduction carries inherent risks. Excessively high nuclei density from ultra-small colloids triggers competitive growth, destabilizes colloidal systems, and impedes Ostwald ripening, ultimately compromising film quality.[43] Meanwhile, the storage stability of the perovskite precursor solution with and without AMPM additive was also investigated, as shown in Fig. S1a–f. After 12 h of aging, the colloidal size of pure perovskite precursor solution and 0.5, 1, 1.5 and 2 mg AMPM-containing perovskite precursor solutions increased to 456, 358, 299, 240 and 156 nm, respectively. Limited variation in colloidal size during 12 h of aging indicates the interactions between AMPM and perovskite inhibit larger aggregation, consequently enhancing precursor solution shelf life.

In addition to colloidal size measurement, the stability of the precursor affected by AMPM was studied by UV-visible spectroscopy. The effect of AMPM on the aging of perovskite precursor solution is shown in Fig. 1c. The pure perovskite
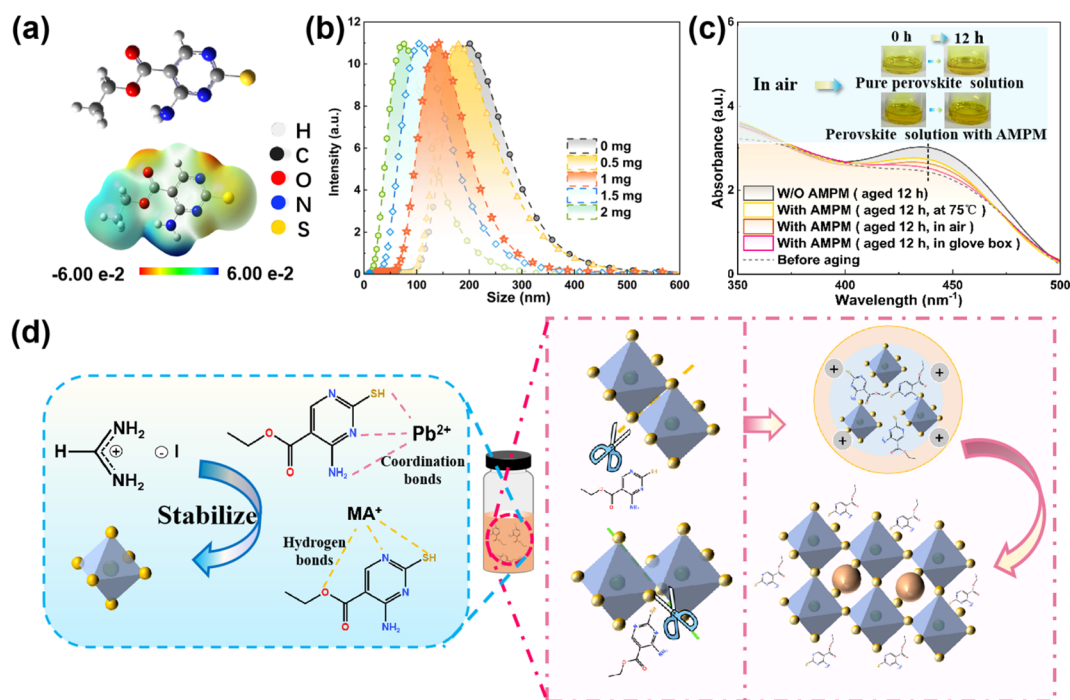


Fig. 1  The molecular structure and ESP of AMPM (a). The colloidal size distributions of control and 0.5−2 mg AMPM-treated perovskite precursor solutions (b). The UV-visible spectra of fresh and 12 h aged perovskite precursor solutions with and without AMPM additive, and images of fresh and 12 h aged perovskite precursor solutions (insets) (c). Schematic diagram showing the mechanism of AMPM's action on perovskite precursors (d).

precursor solution showed marked absorbance increase after 12 h of aging. However, AMPM addition suppressed this change in air at room temperature, in a glove box at 75 °C, and in a glove box at room temperature. A similar stabilizing effect was observed for the UV-visible spectra of $PbI_2$ and MAI in Fig. S1g and h. Compared with pristine $PbI_2$ solution, the $PbI_2$ absorption edge for perovskite precursor solutions containing AMPM showed minimal changes after 12 h of aging. The adsorption peak of MAI solution with AMPM also showed a reduced adsorption during 12 h of aging relative to the bare MAI solution. This suggests that AMPM established effective binding with MAI and $PbI_2$, stabilizing perovskite precursor solution.[15] The fresh and aged perovskite precursor solution images after 12 h are shown as insets in Fig. 1c. The color of pristine perovskite solution after aging for 12 h changed from transparent to light yellow. When AMPM was added into perovskite solution, the color immediately turned dark yellow, suggesting that AMPM interacted with perovskite. After 12 h of aging, the dark yellow color remained stable without further change, further indicating that the addition of AMPM is beneficial for stabilizing perovskite precursor solution. Similar stabilization is visually confirmed for $PbI_2$ and the MAI solutions in Fig. S1h and S1i. These results indicated that AMPM effectively suppresses degradation pathways by forming hydrogen bonds between its –SH, pyrimidine N, and ester groups and $MA^+$, thereby inhibiting deprotonation and subsequent byproduct formation. This contributes to maintaining a stoichiometric balance in the perovskite precursor solution. Meanwhile, AMPM mitigates the reaction between DMSO and $I^-$ by suppressing proton release, thereby significantly extending the shelf life of the solution. Additionally, pyrimidine N, $-NH_2$ and $-SH$ groups in AMPM coordinated with uncoordinated $Pb^{2+}$. Its coordination and hydrogen bonds remove strained non-corner

linkages, simultaneously controlling colloidal assembly towards the desired corner-sharing $[PbI_6]^{4-}$ octahedra and significantly enhancing the stability of perovskite precursor through multifaceted interactions (Fig. 1d). This dual action would establish a more favorable starting point for high-quality perovskite crystallization. A summary table is provided to compare key performance parameters between AMPM and other passivators, including PCE, operational stability, and defect density. As shown in Table S2, AMPM significantly enhances the stability of the perovskite precursor solution compared to other reductive passivators.

$^1$H NMR spectroscopy was employed to elucidate the molecular interactions between the perovskite precursors and AMPM. As depicted in Fig. 2a, when AMPM is mixed with $PbI_2$, the proton signals of $-NH_2$ (7.86 and 8.02 ppm, label yellow color), pyrimidine N (8.48 ppm, label purple color) and $-SH$ (12.64 ppm, label green color) in AMPM shifted significantly to 8.25, 8.37, 8.80, and 13.17 ppm. This observed shift indicated an interaction between the pyrimidine N, $-NH_2$ and $-SH$ of AMPM and uncoordinated $Pb^{2+}$ through coordination bonds. The proton signals of $-CH_3$ and $-CH_2$ groups in the methyl ethyl ester (label orange color) of AMPM remained unchanged. After incorporating AMPM into MAI (Fig. 2b), the chemical shift of the MA cation ($-NH_3^+$) moved downfield from 7.41 to 7.49 ppm. The chemical shift for $-SH$ shifted from 12.64 ppm to 12.63 ppm, that for $-CH_3$ and $-CH_2$ in the methyl ethyl ester moved from 1.26 and 4.23 ppm to 1.20 and 4.17 ppm, and that for pyrimidine N changed from 8.48 ppm to 8.45 ppm. This indicated that $-SH$, pyrimidine N and ester groups can interact with $MA^+$ through hydrogen bonds, decreasing in the dissipation of $MA^+$.[44] The absence of chemical shift alterations for $-NH_2$ implied the predominant interaction with $Pb^{2+}$.
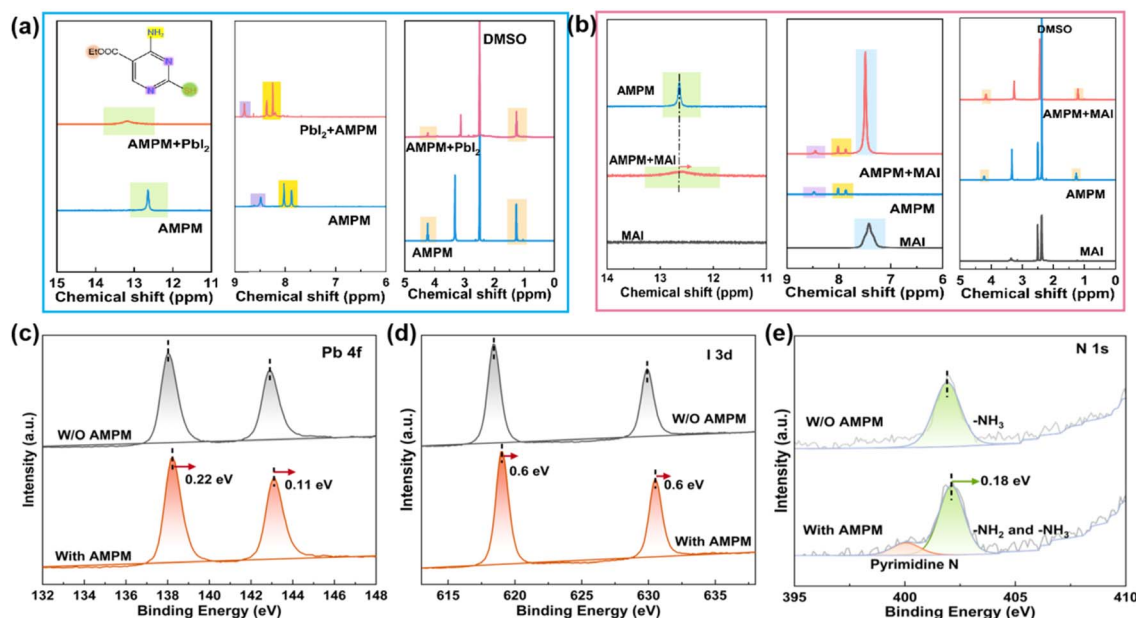


Fig. 2 $^1$H NMR spectra of AMPM and AMPM mixed with $PbI_2$ (a) and MAI (b) dissolved in DMSO-$d_6$ solvent. High-resolution XPS spectra of Pb 4f (c), I 3d (d), and N 1s (e) of original and AMPM-passivated perovskite films.

During perovskite film formation, AMPM remained in the perovskite film to passivate its defects rather than being removed by volatile solvent. FTIR and XPS characterizations were conducted to elucidate the interaction between AMPM and perovskite thin film. The FTIR spectra of AMPM and perovskite without and with AMPM treatment are shown in Fig. S2a. The AMPM spectrum contains characteristic stretching vibrational peaks of –N–H ($3367$ cm$^{-1}$), –SH ($2847$ cm$^{-1}$), C=O ($1707$ cm$^{-1}$), and C–O ($1020$ cm$^{-1}$). For the perovskite film with AMPM treatment, these peaks migrated to 3445 (–N–H), 2857 (–SH), and 1013 (C–O) cm$^{-1}$, and the C=N peak of perovskite shifted from $1564$ cm$^{-1}$ to $1625$ cm$^{-1}$, indicating interactions between AMPM and perovskite.

As shown in Fig. 2c, the Pb 4f XPS spectrum has two peaks at 138.00 eV and 142.89 eV, assigned to Pb 4f$_{5/2}$ and Pb 4f$_{7/2}$, respectively. After AMPM addition, these peaks shifted to 138.22 and 143.00 eV, suggesting that AMPM passivated defects and the formed coordination bonds between AMPM and uncoordinated Pb$^{2+}$.[45] In Fig. 2d, the I 3d peaks in the XPS spectrum (619.00 and 630.49 eV) also shifted toward higher binding energy compared with control film (618.40 and 629.89 eV). This shift was attributed to the interaction of AMPM with MA$^+$ through hydrogen bonds, thereby inhibiting negative charge defects and resulting in a decreased electron density. For N 1s spectra in Fig. 2e, the signal peak at 401.91 eV shifted to higher

binding energy (402.09 eV) after AMPM introduction, implying that AMPM interacted with uncoordinated Pb$^{2+}$ through coordination bonds. These interactions immobilize MA$^+$ and metal ions, thereby suppressing ion migration and stabilizing the perovskite crystal structure. Moreover, the emergence of peaks in N 1s (pyrimidine nitrogen), C 1s (C=O), O 1s, and S 2p XPS spectra confirmed the retention of AMPM in the perovskite film (Fig. S2b–d).

AMPM addition in perovskite precursor solution affected the perovskite thin-film crystal quality. The effect of AMPM on thin-film morphology was investigated using SEM and AFM. As shown in Fig. 3a, the original perovskite film presented a non-uniform, rough texture with distinct grain boundaries. The grain size increased with the AMPM amount up to 1 mg but decreased at 2 mg as shown in Fig. 3b and Fig. S3a–c. The 1 mg AMPM-treated perovskite film displayed a uniform and dense structure with the largest average grain size (220 nm). The average grain size distributions are shown in Fig. S4a–f. This is attributed to AMPM effectively modulating the perovskite precursor, thereby promoting the homogeneous nucleation and grain growth of perovskite crystals. Meanwhile, the 1 mg AMPM-treated film exhibited a lower root mean square (RMS) roughness (28.9 nm $vs.$ 20.2 nm) as shown in Fig. 3c and d.

As shown in Fig. 3e and f, the perovskite film treated with 1 mg AMPM exhibited a lower contact potential difference



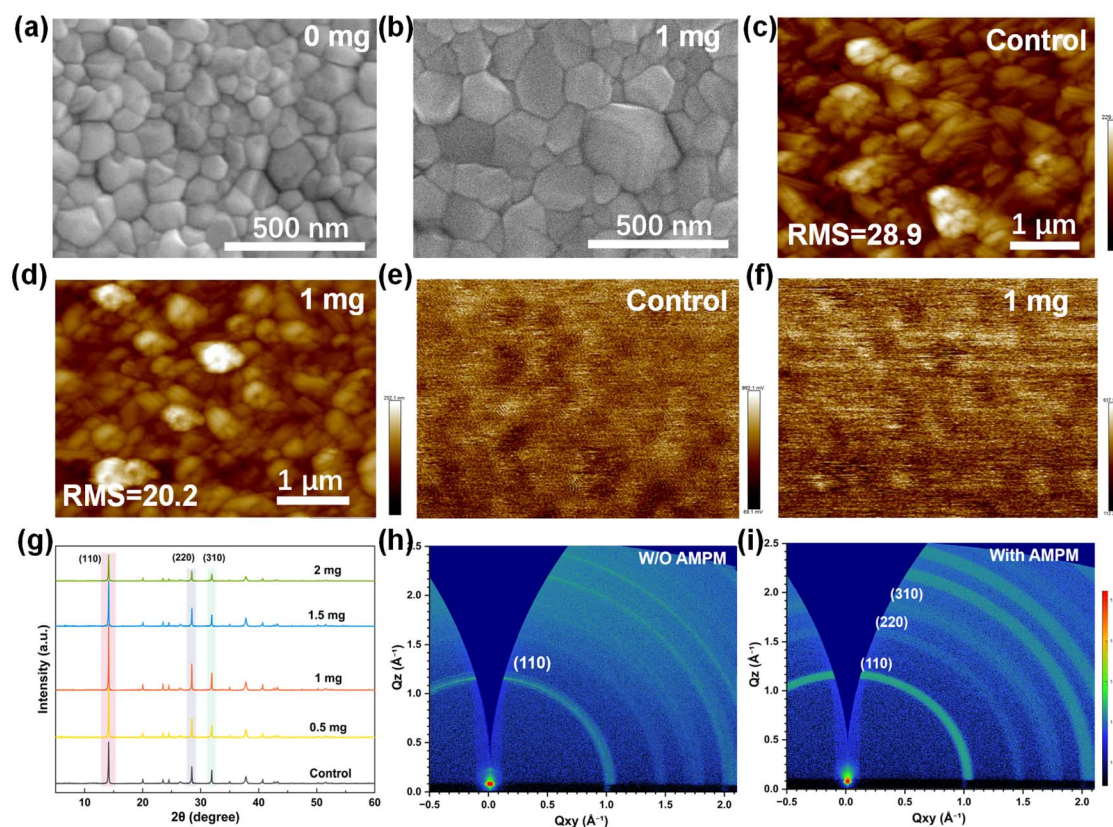Fig. 3 Top-view SEM images of control perovskite film (a) and perovskite film with 1 mg AMPM treatment (b). AFM and KPFM images of the control (c and e) and target perovskite films (d and f). XRD patterns of control and 0.5–2 mg AMPM-treated perovskite films (g). GIWAX patterns for control (h) and 1 mg AMPM-treated (i) perovskite films.

(CPD) (0.402 V) compared to the control film (0.572 V). The lower CPD is related to higher work function and upshift of the Fermi level, boosting interfacial charge extraction and carrier transport.[46–48]

XRD and GIWAXS were systematically performed to explore the influence of AMPM on the perovskite crystallization and crystal orientation. As shown in Fig. 3g and Table S3, the peak intensities of (110), (220) and (310) crystal planes were enhanced after 0.5 mg, 1 mg and 1.5 mg AMPM treatment. The full width at half maximum (FWHM) values of the (110) peak exhibited a significant decrease for these AMPM-treated films. This indicated that AMPM treatment enhanced the crystallinity, with the best improvement observed at 1 mg of AMPM.[49] However, the perovskite film treated with 2 mg AMPM displayed diminished peak intensity and an increased FWHM for the (110) crystal plane. This implied that excessive addition of AMPM to the precursor solution would negatively affect the perovskite crystallization process. The preferential crystal orientation can be quantitatively assessed from the intensity ratios of different crystal planes.[50] The effect of AMPM on crystal orientation was investigated by comparing the change in intensity ratios of (110)/(220), (110)/(310) and (220)/(310). Those ratios increased for AMPM-treated perovskite films (Table S3). Notably, while the (110) plane remained dominant, the film treated with 1 mg AMPM exhibited the smallest relative changes in the (110)/(220) and (110)/(310) ratios, alongside a relatively small change in the (220)/(310) ratio. This indicated that AMPM selectively enhances the relative proportion of higher-Miller-index (220) and (310) planes while maintaining the dominance of the primary (110) facet, confirming facet-specific crystallization modulation as opposed to generalized

crystallinity enhancement. Higher-Miller-index crystal planes exhibit intrinsic self-passivation capability by saturating uncoordinated surface atoms, effectively eliminating gap states from dangling bonds and consequently suppressing defect formation and nonradiative recombination.[51]

As shown in Fig. 3h and i, compared with control film, the AMPM-treated film exhibited a clear and strong diffraction ring, corresponding to the (110) crystal plane. Meanwhile, the intensities of diffraction rings of the (220) and (310) crystal planes were enhanced. The enhancement of these crystal plane diffraction rings suggests that the crystallinity and preferred growth of the crystal planes have been regulated.[52,53] This further demonstrated that AMPM can lead to an apparent preferable growth along (110), (220) and (310). These GIWAXS findings provided reliable corroboration of the XRD results, demonstrating the function of AMPM in manipulating and enhancing the crystalline growth and orientation.

The improvement *via* AMPM treatment of the perovskite film quality inevitably exerts an impact on the photoelectric properties. As shown in Fig. 4a, the perovskite films both with and without AMPM exhibited similar adsorption edges. After AMPM treatment, the adsorption of the perovskite film was improved, which was attributed to the increased crystallinity and reduced defect state density.[40] Accordingly, the intensity of PL was significantly enhanced after AMPM treatment, compared with the pristine perovskite film (Fig. 4b). This suggested that AMPM addition led to fewer defects in the perovskite film. The TRPL spectra are provided in Fig. 4c to quantify the improvement in the perovskite film. The AMPM-treated perovskite film showed a much longer carrier lifetime (123.54 ns), compared with control film (44.13 ns) (Table S4). The longer lifetime indicated
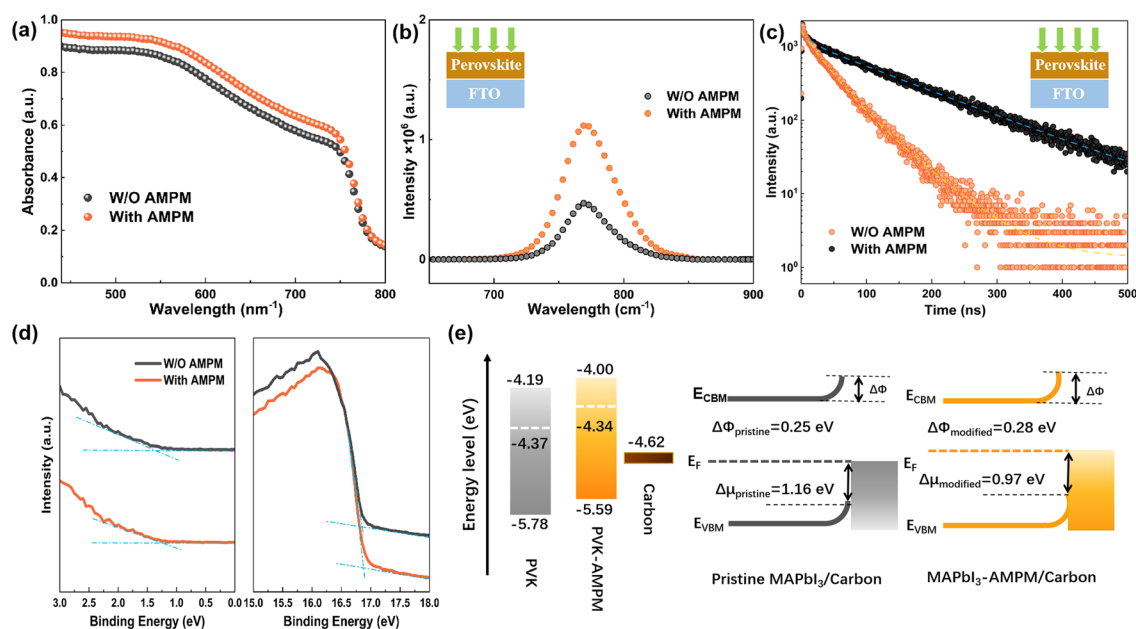


**Fig. 4** UV-visible absorption spectra of perovskite films passivated with and without AMPM treatment (a). PL (b) and TRPL (c) spectra of FTO/perovskite films. UPS energy spectra of secondary electron cutoff region after AMPM treatment and original perovskite film (d). Energy level diagram of original perovskite film and energy level diagram of film after AMPM treatment (e).

that the inhibition of non-radiative recombination was significantly suppressed and the charge extraction kinetics at interfaces was enhanced.[54]

Moreover, electronic property of perovskite films was studied by UPS measurement, and the results are provided in Fig. 4d. The secondary electron cutoff and valence band region were analyzed to determine the work function (WF, calculated as WF $= 21.22 - E_{cutoff}$) and valence band maximum (VBM) position relative to the Fermi level ($E_F$).[55] The control film exhibited a WF of 4.37 eV and a VBM of $-5.78$ eV. After AMPM treatment, the WF decreased to 4.34 eV, while the VBM shifted upwards to $-5.59$ eV (Fig. 4e). The band gap of perovskite was calculated by a Tauc plot, and the results are shown in Fig. S5. Compared with pristine perovskite film ($\Delta\varphi = 0.25$ eV), enhanced upward band bending ($\Delta\varphi = 0.28$ eV) at the perovskite/carbon interface originated from the energy offset ($\Delta\mu$) between the VBM of AMPM-treated perovskite film and WF of the carbon electrode. The higher $\Delta\varphi$ value suggested that AMPM-modified perovskite film suppressed interfacial electron back-transfer to the carbon electrode while facilitating hole extraction, thereby optimizing energy level alignment.[56–58] This is consistent with KPFM results. By optimizing energy levels and establishing a graded

energy structure, AMPM-treated perovskite film exhibited lower CPD. This reduced the electronic barrier and enhanced interfacial electron extraction, thereby improving carrier transport.

HTL-free C-PSCs with FTO/c-TiO₂/m-TiO₂/MAPbI₃/Carbon structure were fabricated to evaluate AMPM's effect on device photovoltaic performance (Fig. 5a). Fig. 5b shows the $J$–$V$ curves of the devices. The control devices showed a champion PCE of 12.44%. The AMPM-treated devices yielded a champion PCE of 16.18%. The detailed photovoltaic parameters are summarized in Table S5. In order to further elevate device efficiency, P3HT was added as the HTL, and the carbon electrode was modified by using TP@Ga. As shown in Fig. S6, the maximum PCE of C-PSCs was further increased to 18.48% using the P3HT HTL and carbon electrode modified by TP@Ga. Fig. 5c shows the resulting changes of PCE, FF, $J_{SC}$, and $V_{OC}$. 0.5–1.5 mg AMPM-modified devices exhibited an enhancement of both FF and $V_{OC}$. This can be attributed to passivation of defects, excellent charge transfer and better energy level alignment. Moreover, the AMPM-modified devices exhibited superior reproducibility, particularly for 1 mg addition of AMPM.

EIS was conducted to investigate the charge transport and carrier recombination properties. As illustrated in Fig. 5d, the
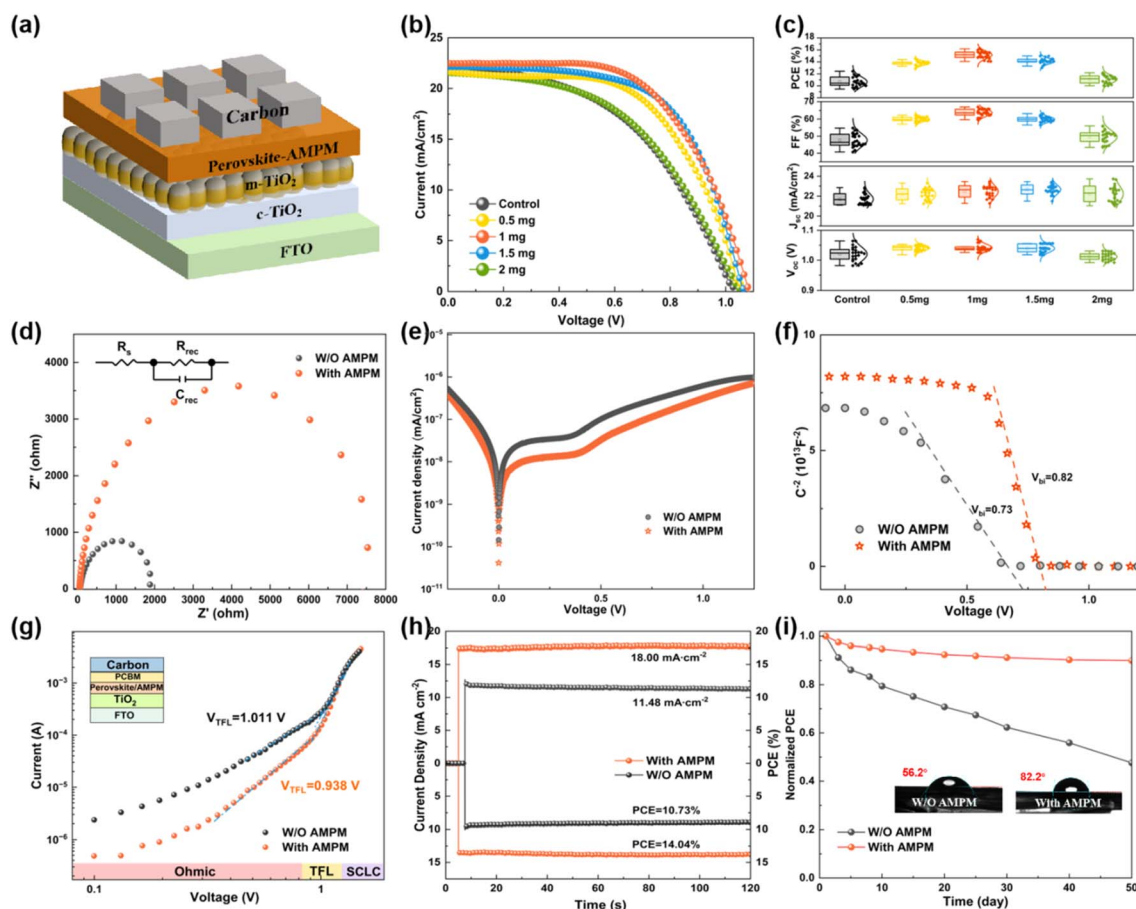


Fig. 5 The device structure (a); $J$–$V$ characteristic curves for different additions of AMPM (b). Box plot of parameters of AMPM-treated device at different concentrations (c). EIS curves (d). Dark current (e). $M$–$S$ curves (f). SCLC of original and AMPM-treated devices (g). Steady-state output curve (h). Long-term stability test at 30–40% humidity of original and AMPM-passivated C-PSCs. Water contact angle of the original and the AMPM-treated perovskite film (i).

charge recombination resistance ($R_{rec}$) of the device treated with AMPM increased from 1870 Ω to 7527 Ω, and the series resistance ($R_s$) was reduced from 11.47 Ω to 6.19 Ω, compared to the control device, indicating suppressed carrier recombination in C-PSCs. The charge transport properties were further investigated by the dark J–V and M–S curves. The reduction of dark current of devices treated by AMPM indicated decreased electrical leakage channels (Fig. 5e). As shown in Fig. 5f, AMPM treatment increased the built-in potential ($V_{bi}$) from 0.73 V to 0.82 V. The elevated $V_{bi}$ enhances the driving force for charge separation within a device.[59] To quantitatively estimate the effect of AMPM on trap density of the perovskite film, SCLC measurement was conducted and the results are shown in Fig. 5g. The AMPM-modified device demonstrated a decreased trap-filled limit voltage ($V_{TFL}$) of 0.938 V and a diminished trap density ($N_t$) of $1.27 \times 10^{16}$ cm$^{-3}$, whereas the control device presented a $V_{TFL}$ of 1.011 V and an $N_t$ of $1.38 \times 10^{16}$ cm$^{-3}$, indicating that the AMPM treatment effectively reduced the defect state density of perovskite. Furthermore, the EQE results in Fig. S7 demonstrated that AMPM-passivated devices had a stronger spectral response between 480 and 800 nm. This suggests that passivated devices have faster charge transfer.[60,61] The spectral response of device is further enhanced by using a P3HT HTL and a carbon electrode modified by TP@Ga. The $J_{SC}$ derived from the EQE spectra indicated that AMPM-treated C-PSCs exhibited enhanced $J_{SC}$.

Given the importance of stability in practical applications of PSCs, the stability of AMPM-modified C-PSCs was studied. As shown in Fig. 5h, the passivated C-PSCs exhibited a steady-state current density of around 18.00 mA cm$^{-2}$ and a steady-state PCE of 14.04% at 0.785 V, whereas the control devices had values of 11.48 mA cm$^{-2}$ and 10.73% at 0.710 V. For the long-term stability results in Fig. 5i, after 50 days of storage at room temperature (30–40% relative humidity), AMPM-passivated C-PSCs retained 90% of their initial PCE, while the control C-PSCs retained only 47% As shown in Fig. S8, PbI$_2$ peak intensity of control film increased significantly after 50 days. With AMPM treatment, the long-term stability of films was slightly improved and the PbI$_2$ diffraction peaks were hardly detected for the AMPM-modified film after 50 days. This confirmed that the AMPM-mediated defect suppression substantially extends C-PSC operational lifetimes under environmental stressors. Moreover, the water contact angle of AMPM-modified film is 82.2°, greater than that of pristine film (56.2°) (Fig. 5i).

## 4. Conclusion

In summary, a feasible strategy was proposed to stabilize perovskite precursor and regulate its crystallization growth using a multifunctional passivator, AMPM. AMPM with functional groups of NH$_2$, –SH, ester and pyrimidine N can interact with precursors MAI and PbI$_2$ through coordination and hydrogen bonds, respectively. The results of DLS and UV-visible spectroscopy of perovskite precursor solution demonstrated that these chemical interactions effectively dissociate face- and edge-shared $[PbI_6]^{4-}$ octahedral aggregates, enhancing precursor colloidal dispersion, improving precursor stability

and driving the reorganization into corner-shared $[PbI_6]^{4-}$. This restructuring significantly enhanced the dispersion and stability of the precursor solution. Moreover, XRD and GIWAXS results revealed that AMPM preferentially increased the relative abundance of higher-Miller-index (220) and (310) planes while preserving the predominance of the primary (110) facet, thereby reducing perovskite defect state density and improving charge extraction. PL and TRPL further confirm that AMPM significantly reduced defect state density and improved interface hole transport. Consequently, the PCE of AMPM-treated C-PSCs increased markedly from 12.44% to 16.18%. The champion PCE of C-PSCs was further increased to 18.48% using a P3HT HTL and a TP@Ga-modified carbon electrode. After 50 days of storage at room temperature and a relative humidity of 30–40%, the long-term stability of AMPM-treated C-PSCs remained at 90% of the initial PCE. This study successfully establishes a multi-site anchoring passivator as a powerful and versatile approach for concurrently stabilizing perovskite precursor solution and regulating crystallization dynamics. This dual-action strategy paves the way for the fabrication of high-performance, solution-processed perovskite optoelectronic devices with enhanced reproducibility and stability.

## Author contributions

Mengqi Geng: conceptualization; data curation; formal analysis; investigation; methodology; visualization; writing-original draft; writing-review & editing, Jialiang Li: investigation-supporting; Ke Wang: investigation-supporting, Le Jiang: investigation-supporting, Dan Lu: investigation-supporting, Shoaib Iqbal: investigation-supporting, Yu Gu: investigation-supporting, Lixin Chen: investigation-supporting, Tingting Xu: conceptualization; data curation; formal analysis; funding acquisition; methodology; project administration; resources; supervision; visualization; writing-original draft; writing-review & editing.

## Conflicts of interest

There are no conflicts to declare.

## Data availability

The data are available from the corresponding author on reasonable request.

Supplementary information: Fig. S1–S8 (showing DLS images, UV-vis absorption spectra, the FTIR spectra, XPS spectra of C 1s, O 1s, and S 2p, SEM images, grain size distribution, Tauc plot, J–V curves, EQE curves, and XRD spectra); Tables S1–S5 (the colloidal size of perovskite precursor solution, summary of key photovoltaic parameters of various passivators, the full width at half maximum, fitting parameters of lifetime from TRPL, summary of photovoltaic parameters of C-PSCs); and additional references. See DOI: https://doi.org/10.1039/d5sc05095b.

## Acknowledgements

## References

1 D. Bogachuk, S. Zouhair, K. Wojciechowski, B. Yang, V. Babu, L. Wagner, B. Xu, J. Lim, S. Mastroianni, H. Pettersson, A. Hagfeldt and A. Hinsch, Low-Temperature Carbon-Based Electrodes in Perovskite Solar Cells, *Energy Environ. Sci.*, 2020, **13**, 3880–3916.

2 C. Zuo, H. J. Bolink, H. Han, J. Huang, D. Cahen and L. Ding, Advances in Perovskite Solar Cells, *Adv. Sci.*, 2016, **3**, 1500324.

3 L. M. González, D. Ramirez and F. Jaramillo, Current Status and Trends of Carbon-Based Electrodes for Fully Solution-Processed Perovskite Solar Cells, *J. Energy Chem.*, 2022, **68**, 222–246.

4 W. Peng, Y. Zhang, X. Zhou, J. Wu, D. Wang, G. Qu, J. Zeng, Y. Xu, B. Jiang, P. Zhu, Y. Du, Z. Li, X. Lei, Z. Liu, L. Yan, X. Wang and B. Xu, A Versatile Energy-Level-Tunable Hole-Transport Layer for Multi-Composition Inverted Perovskite Solar Cells, *Energy Environ. Sci.*, 2025, **18**, 874–883.

5 S.-H. Turren-Cruz, M. Saliba, M. T. Mayer, H. Juárez-Santiesteban, X. Mathew, L. Nienhaus, W. Tress, M. P. Erodici, M.-J. Sher, M. G. Bawendi, M. Grätzel, A. Abate, A. Hagfeldt and J.-P. Correa-Baena, Enhanced Charge Carrier Mobility and Lifetime Suppress Hysteresis and Improve Efficiency in Planar Perovskite Solar Cells, *Energy Environ. Sci.*, 2018, **11**, 78–86.

6 T. Ji, Y.-K. Wang, L. Feng, G.-H. Li, W.-Y. Wang, Z.-F. Li, Y.-Y. Hao and Y.-X. Cui, Charge Transporting Materials for Perovskite Solar Cells, *Rare Met.*, 2021, **40**, 2690–2711.

7 M. Cheng, C. Zuo, Y. Wu, Z. Li, B. Xu, Y. Hua and L. Ding, Charge-Transport Layer Engineering in Perovskite Solar Cells, *Sci. Bull.*, 2020, **65**, 1237–1241.

8 A. Kojima, K. Teshima, Y. Shirai and T. Miyasaka, Organometal Halide Perovskites as Visible-Light Sensitizers for Photovoltaic Cells, *J. Am. Chem. Soc.*, 2009, **131**, 6050–6051.

9 M. A. Green, E. D. Dunlop, M. Yoshita, N. Kopidakis, K. Bothe, G. Siefer, X. Hao and J. Y. Jiang, Solar Cell Efficiency Tables (Version 66), *Prog. Photovoltaics Res. Appl.*, 2025, **33**, 795–810.

10 K. Yan, M. Long, T. Zhang, Z. Wei, H. Chen, S. Yang and J. Xu, Hybrid Halide Perovskite Solar Cell Precursors: Colloidal Chemistry and Coordination Engineering behind Device Processing for High Efficiency, *J. Am. Chem. Soc.*, 2015, **137**, 4460–4468.

11 L. Chao, T. Niu, W. Gao, C. Ran, L. Song, Y. Chen and W. Huang, Solvent Engineering of the Precursor Solution toward Large-Area Production of Perovskite Solar Cells, *Adv. Mater.*, 2021, **33**, 2005410.

12 X. Wei, M. Zhang, X. Liu, F. Chen, X. Lei, H. Liu, F. Meng, H. Zeng, S. Yang and J. Liu, Semitransparent $CH_3NH_3PbI_3$ Films Achieved by Solvent Engineering for Annealing- and Electron Transport Layer-Free Planar Perovskite Solar Cells, *Sol. RRL*, 2018, **2**, 1700222.

13 Z. Huang, Z. Ma, C. Deng, T. Yu, G. Li, Z. Du, W. You, J. Yang, Y. Chen, Y. Li, S. Hou, Q. Yang, Q. Zhang, H. Du, Y. Li, H. Shu, Q. Liu, C. Peng, Y. Huang, J. Yu, Y. Lin, K. Sun and W. Long, Aging-Resistant Precursor with Ultrawide Annealing Window for 24.08% Perovskite Solar Cells, *Adv. Energy Mater.*, 2024, **14**, 2302769.

14 Y. Jiang, H.-Q. Du, R. Zhi, M. U. Rothmann, Y. Wang, C. Wang, G. Liang, Z.-Y. Hu, Y.-B. Cheng and W. Li, Eliminating Non-Corner-Sharing Octahedral for Efficient and Stable Perovskite Solar Cells, *Adv. Mater.*, 2024, **36**, 2312157.

15 N. Wu, T. Yang, Z. Wang, Y. Wu, Y. Wang, C. Ma, H. Li, Y. Du, D. Zhao, S. Wang, P. Liu, W. Huang, X. Ren, S. Liu and K. Zhao, Stabilizing Precursor Solution and Controlling Crystallization Kinetics Simultaneously for High-Performance Perovskite Solar Cells, *Adv. Mater.*, 2023, **35**, 2304809.

16 F. Yang, M. A. Kamarudin, D. Hirotani, P. Zhang, G. Kapil, C. H. Ng, T. Ma and S. Hayase, Melamine Hydroiodide Functionalized $MAPbI_3$ Perovskite with Enhanced Photovoltaic Performance and Stability in Ambient Atmosphere, *Sol. RRL*, 2019, **3**, 1800275.

17 Y. Ma, H. Cai, Y. Liu, B. He, H. Zhang, Y. Cheng, G. Liu, J. Zhao, Y.-B. Cheng and J. Zhong, Alleviation of Precursor Degradation Induced by DMF/DMSO Mixture for Enhanced Performance of Perovskite Solar Cells, *Angew. Chem., Int. Ed.*, 2025, **64**, e202504253.

18 C. Pereyra, H. Xie and M. Lira-Cantu, Additive Engineering for Stable Halide Perovskite Solar Cells, *J. Energy Chem.*, 2021, **60**, 599–634.

19 D.-N. Lee, Y.-S. Jeon, S. C. Cho, S. U. Lee and N.-G. Park, Additive Engineering in Perovskite Solar Cells: Effect of Basicity of Benzoquinone Additives Controlled by Substituent, *ACS Energy Lett.*, 2024, **9**, 4172–4179.

20 J. Zhang, W. Sun, J. Wu, J. Liu, S. Tang, Y. Xie, C. Lu and F. Yu, Macrocyclic Thiol Ligand Additive Engineering for Stable and Efficient Perovskite Solar Cells, *Chem. Eng. J.*, 2024, **494**, 152978.

21 B. Chen, P. N. Rudd, S. Yang, Y. Yuan and J. Huang, Imperfections and Their Passivation in Halide Perovskite Solar Cells, *Chem. Soc. Rev.*, 2019, **48**, 3842–3867.

22 T. Li, Y. Pan, Z. Wang, Y. Xia, Y. Chen and W. Huang, Additive Engineering for Highly Efficient Organic–Inorganic Halide Perovskite Solar Cells: Recent Advances and Perspectives, *J. Mater. Chem. A*, 2017, **5**, 12602–12652.

23 Z. Wu, S. R. Raga, E. J. Juarez-Perez, X. Yao, Y. Jiang, L. K. Ono, Z. Ning, H. Tian and Y. Qi, Improved Efficiency and Stability of Perovskite Solar Cells Induced by C=O Functionalized Hydrophobic Ammonium-Based Additives, *Adv. Mater.*, 2018, **30**, 1703670.

24 Y. Lin, L. Shen, J. Dai, Y. Deng, Y. Wu, Y. Bai, X. Zheng, J. Wang, Y. Fang, H. Wei, W. Ma, X. C. Zeng, X. Zhan and

J. Huang, π-Conjugated Lewis Base: Efficient Trap-Passivation and Charge-Extraction for Hybrid Perovskite Solar Cells, *Adv. Mater.*, 2017, **29**, 1604545.

25 Y. Zhao, J. Wei, H. Li, Y. Yan, W. Zhou, D. Yu and Q. Zhao, A Polymer Scaffold for Self-Healing Perovskite Solar Cells, *Nat. Commun.*, 2016, **7**, 10228.

26 X. Li, M. Ibrahim Dar, C. Yi, J. Luo, M. Tschumi, S. M. Zakeeruddin, M. K. Nazeeruddin, H. Han and M. Grätzel, Improved Performance and Stability of Perovskite Solar Cells by Crystal Crosslinking with Alkylphosphonic Acid ω-Ammonium Chlorides, *Nat. Chem.*, 2015, **7**, 703–711.

27 H. Zheng, L. Zhu, L. Hu, S. Yang, S. Chen, A. Alsaedi, T. Hayat, Y. Huang, X. Pan and S. Dai, Promoting Perovskite Crystal Growth to Achieve Highly Efficient and Stable Solar Cells by Introducing Acetamide as an Additive, *J. Mater. Chem. A*, 2018, **6**, 9930–9937.

28 Y.-J. Kang, S.-N. Kwon, S.-P. Cho, Y.-H. Seo, M.-J. Choi, S.-S. Kim and S.-I. Na, Antisolvent Additive Engineering Containing Dual-Function Additive for Triple-Cation p–i–n Perovskite Solar Cells with over 20% PCE, *ACS Energy Lett.*, 2020, **5**, 2535–2545.

29 Y. Gou, W. Dai, X. Xie, J. Zhang, W. Li, B. Jin, Q. Tai, X. Wang and J. Li, Suppressing Deprotonation to Extend the Shelf Life of Perovskite Precursor Solutions and Enhance the Stability and Efficiency of Perovskite Solar Cells, *Adv. Funct. Mater.*, 2025, **30**, 2505965.

30 W. Hu, J. Yang, C. Yang, X. Xiao, C. Wang, Z. Cui, Q. Gao, J. Qi, M. Xia, Y. Su, A. Mei and H. Han, Stabilizing Perovskite Precursors with the Reductive Natural Amino Acid for Printable Mesoscopic Perovskite Solar Cells, *J. Energy Chem.*, 2024, **90**, 32–39.

31 S. Yin, X. Jiao, X. Liu, M. Liu, B. Xu, N. Li, Y. Lu, S. Yang and W. Kong, Synergistic Effect of H+ and I− Oxidation Enables Long-Term Stability of the Precursor Solutions and Enhanced Performance of FA-Dominated Perovskite Solar Cells, *Adv. Funct. Mater.*, 2024, **34**, 2411183.

32 C. Tian, T. Wu, Y. Zhao, X. Zhou, B. Li, X. Han, K. Li, C. Hou, Y. Li, H. Wang and Q. Zhang, Anion-Stabilized Precursor Inks Toward Efficient and Reproducible Air-Processed Perovskite Solar Cells, *Adv. Energy Mater.*, 2024, **14**, 2303666.

33 G. G. Jeon, S. E. Yoon, J. Han, H. W. Chun, S. J. Shin, M. J. Choi, S. U. Park, S.-J. Ko, S. Huang, N. Park, J. H. Kim and J. Kim, Surfactant-Assisted Colloidal Size and Charge Control in Perovskite Solutions for High-Performance and Stable Solar Cells, *Chem. Eng. J.*, 2025, **519**, 164991.

34 H. Wang, M. Zhang, J. Miao, B. Li, Y. Liu, Y. Zhang, Y. Chen, W. Pu, M. Li and S. Yun, Enhanced Homogeneity in Perovskite Photovoltaic Films *via* Antisolvent Extraction of a Methylamine-Based Gel Precursor, *ACS Appl. Mater. Interfaces*, 2024, **16**, 55407–55415.

35 M. Geng, Y. Li, Y. Wang, J. Li, D. Lu, L. Jiang, Q. Meng and T. Xu, Rational Design of Pyridine Bidentate Molecules for Surface Passivating Carbon-Based Perovskite Solar Cells, *Chem. Eng. J.*, 2025, **510**, 161648.

36 D. Lu, M. Geng, X. Ma, Y. Gu, J. Li, J. Mao, L. Jiang, J. Chen and T. Xu, Natural Polyphenol-Assisted Dispersing Liquid Metal/Carbon Composite Electrode for the Superior Interface in Carbon-Based Perovskite Solar Cells, *Langmuir*, 2025, **41**, 11113–11122.

37 Z. Yang, A. Sun, Y. Ren, Z. Li, L. e. Mo, H. Zhang, Y. Huang and L. Hu, Stabilize Perovskite Precursors and Inhibit Intermediates for High Performing Perovskite Solar Cells, *Small*, 2025, **21**, 2503279.

38 W. Tang, Y. Chen, R. Shi, Y. Wu and J. Zhang, Extending The Shelf-Life of Precursor Solutions and Inhibiting Light-Induced Oxidation of Iodides for Achieving Highly Efficient and Durable Perovskite Solar Cells, *J. Mater. Chem. A*, 2025, **13**, 19569–19579.

39 G. Hu, Z. Zhao, Y. Shen, Y. Wang and D. Yang, Cation and Octahedral Synergistic Regulation for Stable FAPbI$_3$ Perovskite Solar Cells, *Small*, 2025, **21**, 2502025.

40 L. Meng, Q. Wei, Z. Yang, D. Yang, J. Feng, X. Ren, Y. Liu and S. Liu, Improved Perovskite Solar Cell Efficiency by Tuning the Colloidal Size and Free Ion Concentration in Precursor Solution using Formic Acid Additive, *J. Energy Chem.*, 2020, **41**, 43–51.

41 Y. Yang, J. Wu, X. Wang, Q. Guo, X. Liu, W. Sun, Y. Wei, Y. Huang, Z. Lan, M. Huang, J. Lin, H. Chen and Z. Wei, Suppressing Vacancy Defects and Grain Boundaries *via* Ostwald Ripening for High-Performance and Stable Perovskite Solar Cells, *Adv. Mater.*, 2020, **32**, 1904347.

42 D. P. McMeekin, Z. Wang, W. Rehman, F. Pulvirenti, J. B. Patel, N. K. Noel, M. B. Johnston, S. R. Marder, L. M. Herz and H. J. Snaith, Crystallization Kinetics and Morphology Control of Formamidinium–Cesium Mixed-Cation Lead Mixed-Halide Perovskite *via* Tunability of the Colloidal Precursor Solution, *Adv. Mater.*, 2017, **29**, 1607039.

43 M. Azam, S. Yue, K. Liu, Y. Sun, J. Liu, K. Ren, Z. Wang, S. Qu and Z. Wang, Insights on The Correlation of Precursor Solution, Morphology of the Active Layer and Performance of the Perovskite Solar Cells, *J. Alloys Compd.*, 2018, **731**, 375–380.

44 T. Yong, S. Choi, S.-K. Kim, S. Han, G. Seo, H. J. Kim, J. Y. Park, H. N. Yu, H. R. You, E. J. Lee, G. Lee, W. Lee, S. Kim, S. Yun, Y. Lee, J. Lee, D.-H. Kim, S. J. Lim, D.-H. Nam, Y. Kim, J. Lim, B. J. Moon and J. Choi, Hydrogen Bond-Mediated Pseudo-Halide Complexation for Stable and Efficient Perovskite Precursors and Solar Cells, *Energy Environ. Sci.*, 2024, **17**, 9443–9454.

45 S. Riaz, M. Liu, Z. Zhong, H. Mi, W. Zheng, Y. Xiao, Y. Qi, M. S. Qureshi, S. Umar and Y. Xie, Enhancing Efficiency and Stability in Carbon-Based Perovskite Solar Cells through Dual-Interface Modification, *J. Power Sources*, 2025, **630**, 236133.

46 X. Hu, Y. Pan, J. Wang, Z. Liu and W. Chen, Reducing Energy Disorder by Stabilizing Octahedral Lattice with Thiocyanate for Efficient and Stable Sn-Pb Mixed Perovskite Solar Cells, *Nano Energy*, 2023, **118**, 108937.

47 Z. Lan, H. Huang, Y. Lu, S. Qu, M. Wang, S. Du, Y. Yang, C. Sun, Q. Zhang, Y. Suo, X. Wang, L. Yan, P. Cui, Z. Zhao and M. Li, Homogenizing the Electron Extraction *via* Eliminating Low-Conductive Contacts Enables Efficient

Perovskite Solar Cells with Reduced Up-Scaling Losses, *Adv. Funct. Mater.*, 2024, **34**, 2316591.

48 M. B. Faheem, B. Khan, Y. Zhang, H. Li, M. Saud, H. Lin, H. Zhang, S. B. Ahmed, V. Vanshika, R. Qiao, P. Kaswekar, Y. Wang, W. Zheng, J.-H. He and Q. Qiao, Synergistic Solvent and Surface Engineering to Reduce $V_{OC}$ Loss in Tin Halide Perovskite Solar Cells, *ACS Energy Lett.*, 2025, **17**, 3337–3348.

49 M. Wang, Y. Yin, W. Cai, J. Liu, Y. Han, Y. Feng, Q. Dong, Y. Wang, J. Bian and Y. Shi, Synergetic Co-Modulation of Crystallization and Co-Passivation of Defects for FAPbI$_3$ Perovskite Solar Cells, *Adv. Funct. Mater.*, 2022, **32**, 2108567.

50 J. Chang, E. Feng, H. Li, Y. Ding, C. Long, Y. Gao, Y. Yang, C. Yi, Z. Zheng and J. Yang, Crystallization and Orientation Modulation Enable Highly Efficient Doctor-Bladed Perovskite Solar Cells, *Nano-Micro Lett.*, 2023, **15**, 164.

51 S. Li, Y. Xiao, R. Su, W. Xu, D. Luo, P. Huang, L. Dai, P. Chen, P. Caprioglio, K. A. Elmestekawy, M. Dubajic, C. Chosy, J. Hu, I. Habib, A. Dasgupta, D. Guo, Y. Boeije, S. J. Zelewski, Z. Lu, T. Huang, Q. Li, J. Wang, H. Yan, H.-H. Chen, C. Li, B. A. I. Lewis, D. Wang, J. Wu, L. Zhao, B. Han, J. Wang, L. M. Herz, J. R. Durrant, K. S. Novoselov, Z.-H. Lu, Q. Gong, S. D. Stranks, H. J. Snaith and R. Zhu, Coherent Growth of High-Miller-Index Facets Enhances Perovskite Solar Cells, *Nature*, 2024, **635**, 874–881.

52 S. Yuan, T. Zhang, H. Chen, Y. Ji, Y. Hao, H. Zheng, Y. Wang, Z. David Chen, L. Chen and S. Li, Dual-Functional Passivators for Highly Efficient and Hydrophobic FA-Based Perovskite Solar Cells, *Chem. Eng. J.*, 2022, **433**, 133227.

53 Y. Qiang, X. Zheng, W. Sharmoukh, H. Cao, Y. Li, J. Li, L. Zhao, Y. Chen, Y. Wei, Y. Gao, Y. Yang and Z. Yu, Side-Chain Engineering of Nickel Naphthalocyanine-Based Hole-Transport Materials Realizes >25% Efficiency and Light-Heat Durable Perovskite Solar Cells, *Adv. Funct. Mater.*, 2025, 2507865.

54 D. Lu, J. Fan, X. Ma, M. Geng, J. Li and T. Xu, Dual-Functional Passivation Agent of Natural Dye Congo Red for Enhanced Carbon-Based Perovskite Solar Cells, *ACS Appl. Mater. Interfaces*, 2024, **16**, 69439–69449.

55 S. Dai, H. Cao, W. Sharmoukh, Y. Qiang, L. Zhao, Y. Chen, Y. Li, H. Nasser Abdelhamid, N. Taghavinia and Z. Yu, Pure-Phase Two-Dimensional Perovskite Capping Layer Enables High-performance and Durable Carbon-Based Photovoltaics, *Chem. Eng. J.*, 2024, **497**, 154611.

56 J. Li, C. Shi, M. Geng, J. Mao, L. Jiang, D. Lu and T. Xu, Constructing Type-II Band Alignment of 3D/2D Heterojunction for Improved Carrier Transport in Carbon-Based Perovskite Solar Cells, *ACS Appl. Mater. Interfaces*, 2025, **17**, 22831–22840.

57 Y. Zou, W. Yu, H. Guo, Q. Li, X. Li, L. Li, Y. Liu, H. Wang, Z. Tang, S. Yang, Y. Chen, B. Qu, Y. Gao, Z. Chen, S. Wang, D. Zhang, Y. Chen, Q. Chen, S. M. Zakeeruddin, Y. Peng, H. Zhou, Q. Gong, M. Wei, M. Grätzel and L. Xiao, A Crystal Capping Layer for Formation of Black-Phase FAPbI$_3$ Perovskite in Humid Air, *Science*, 2024, **385**, 161–167.

58 X. Zhang, F. Liu, Y. Guan, Y. Zou, C. Wu, D. Shi, H. Zhang, W. Yu, D. Zou, Y. Zhang, L. Xiao and S. Zheng, Reducing the Voc Loss of Hole Transport Layer-Free Carbon-Based Perovskite Solar Cells *via* Dual Interfacial Passivation, *Nano-Micro Lett.*, 2025, **17**, 258.

59 K. Zou, Q. Li, J. Fan, H. Tang, L. Chen, S. Tao, T. Xu and W. Huang, Pyridine Derivatives' Surface Passivation Enables Efficient and Stable Carbon-Based Perovskite Solar Cells, *ACS Mater. Lett.*, 2022, **4**, 1101–1111.

60 R. Wang, J. Zhu, J. You, H. Huang, Y. Yang, R. Chen, J. Wang, Y. Xu, Z. Gao, J. Chen, B. Xu, B. Wang, C. Chen, D. Zhao and W. Zhang, Custom-Tailored Solvent Engineering for Efficient Wide-Bandgap Perovskite Solar Cells with A Wide Processing Window and Low $V_{OC}$ Losses, *Energy Environ. Sci.*, 2024, **17**, 2662–2669.

61 N. Yan, Y. Cao, Z. Dai, L. Jiang, Y. Yang, T. Li, L. Li, S. Liu, Z. Fang and J. Feng, Heterogeneous Seed-Assisted FAPbI$_3$ Crystallization for Efficient Inverted Perovskite Solar Cells, *Energy Environ. Sci.*, 2024, **17**, 5070–5079.